Letter

Generalized Fourier's law in mesoscopic systems

Luciano C. Lapas *

Latin American Institute of Life and Natural Sciences, Universidade Federal da Integração Latino-Americana, Avenida Tancredo Neves, 6731, Bloco 6, Espaço 3, Sala 5, Foz do Iguaçu 85867-970, Paraná, Brazil

(Received 21 June 2026; accepted 4 November 2026; published 13 November 2026)

Fourier's law fails when the mean free path of the energy carriers becomes comparable to the length scales and timescales over which the temperature field varies. We derive a thermodynamically consistent generalization in which the conductivity becomes a nonlocal memory operator $\boldsymbol{\kappa}_{\rm eff}(\mathbf{k}, \omega)$, by combining mesoscopic nonequilibrium thermodynamics with the Mori-Kubo–Zwanzig projection-operator formalism. The Onsager kernel is a tensor sum over vibrational normal modes weighted by their Bose heat capacities and relaxation functions; it satisfies the second law for any closure consistent with the fluctuation-dissipation theorem and reduces, in the relaxation-time closure, to the nonlocal conductivity of the phonon Boltzmann equation. Two consequences follow. First, direction-dependent sampling of this tensor in a pump-probe experiment makes a nominally isotropic crystal exhibit apparent conductivities $\Lambda_z \neq \Lambda_r$. Second, the modulation frequency does not introduce temporal memory but sets the probed wave vector through the thermal penetration depth, so that the frequency-dependent suppression of the apparent conductivity measured by time-domain thermoreflectance on Ge and SiGe alloys is a spatial-nonlocality effect, with effective lengths of 0.25–0.4 μm. With published mean-free-path spectra and no parameter adjusted to the thermoreflectance data, the kernel reproduces the spot-size dependence of Si, the frequency dependence of the apparent conductivity of Ge and $Si_{0.2}Ge_{0.8}$, and the rise of the apparent interface conductance of $Al/Si_{0.99}Ge_{0.01}$, and contains the two-channel ballistic/diffusive model as a two-sector projection.

DOI: 10.1103/ggz5-nggb

Introduction. The classical theory of heat conduction rests on Fourier's law,

$$\mathbf{J}_q = -\kappa \nabla T, \tag{1}$$

relating the heat flux $\mathbf{J}_q$ to the local temperature gradient through a scalar conductivity κ. Equation (1) is accurate whenever the carrier mean free path (MFP) ℓ_c is far shorter than the experimental length scale $L_{\rm exp}$, i.e., in the diffusive regime where the Knudsen number $\mathrm{Kn} \equiv \ell_c / L_{\rm exp} \ll 1$ and carriers (e.g., phonons in dielectrics and most semiconductors, electrons in metals [1,2]) relax to local equilibrium much faster than the macroscopic field evolves. Local energy conservation then yields the diffusion equation $\partial_t T = a\, \nabla^2 T$ [3,4], with a the thermal diffusivity, and a localized pulse spreads into a Gaussian profile whose width grows as $2\sqrt{at}$. This description breaks down when

*Contact author: luciano.lapas@unila.edu.br

Published by the American Physical Society under the terms of the Creative Commons Attribution 4.0 International license. Further distribution of this work must maintain attribution to the author(s) and the published article's title, journal citation, and DOI.

L_{exp} is no longer large compared with the longest active MFP, as in nanostructures [5], colloids [6], and biological organelles [7], where $\mathrm{Kn} \gtrsim \mathcal{O}(1)$ marks the onset of nonlocal, partially ballistic transport [2,8]. Quantitative evidence is now abundant: quasiballistic transport and size-dependent effective conductivity in silicon membranes [9]; the anisotropic failure of Fourier's law in time-domain thermoreflectance (TDTR) on Si and SiGe [10]; and non-Gaussian temperature profiles in translucent polymers and glasses, where internal infrared radiation provides an additional transport channel with millimeter-scale effective MFPs [11].

These breakdowns are not all of the same kind, and a useful theory must distinguish them. The general constitutive response is nonlocal in both time and space, but a given experiment probes one axis preferentially. In TDTR, the relevant timescale $1/f$ is far longer than carrier lifetimes, so temporal memory is negligible and the modulation frequency f acts only by fixing a spatial scale, the thermal penetration depth $d_p = \sqrt{\kappa_{\mathrm{ref}}/\pi C f}$, with C the volumetric heat capacity [10] and κ_{ref} a fixed reference conductivity (the bulk value below); the same holds for the macroscale radiative anomaly of Ref. [11]. Temporal memory dominates instead in second-sound experiments, whereas room-temperature transient gratings, like TDTR, probe spatial nonlocality [12]. The TDTR breakdown is moreover *anisotropic*: Beam-offset measurements on nominally isotropic Si return distinct through-plane and in-plane conductivities, $\Lambda_z \approx 140\ \mathrm{W\,m^{-1}\,K^{-1}}$ and $\Lambda_r \approx 80\ \mathrm{W\,m^{-1}\,K^{-1}}$ [10,13], and it is interface mediated, requiring a nonequilibrium resistance beyond a local boundary conductance [10]. Following Wilson and Cahill, we use Λ_A, Λ_z, and Λ_r to denote *apparent* conductivities extracted by fitting TDTR data with local diffusive models, while κ_{bulk} denotes the intrinsic bulk conductivity in the Fourier limit. Related nonlocal approaches include phonon Boltzmann transport equation (BTE) kernels in the relaxation-time approximation [14–17] and beyond it [18], applied to TDTR analytically [15,19], through mean-free-path spectroscopy [20], by Monte Carlo [21], or with measured interfacial transmissivities [22]; Guyer-Krumhansl hydrodynamic analyses [23,24]; two-channel interface models [25]; and, closest to the present work, a spatiotemporal Green-Kubo kernel obtained by Zwanzig projection and realized for phonons through the linearized BTE [26]. The kinetic treatments start from a prescribed collision operator, so that their second law and exponential memory are those of that operator, and the interface enters them through a boundary condition, fitted rates, or a separable kernel with illustrative parameters. The constitutive law derived here starts instead from mesoscopic entropy production and the Mori-Kubo-Zwanzig identity: It guarantees non-negative entropy production for any closure consistent with the fluctuation-dissipation theorem, recovers the BTE and Guyer-Krumhansl kernels as Markovian and single-pole limits of a memory function that obeys this theorem, and, given a modal boundary condition, yields the interfacial nonequilibrium resistance from the same kernel, the two-channel model [25] being its two-sector projection (Sec. SIX of the Supplemental Material [27]).

In this Letter, we derive this constitutive law. Combining mesoscopic nonequilibrium thermodynamics (MNET) [35–37] with the Mori-Kubo-Zwanzig projection-operator formalism [38–41] promotes the conductivity to a nonlocal memory operator $\boldsymbol{\kappa}_{\mathrm{eff}}(\mathbf{k}, \omega)$ whose Onsager kernel decomposes into vibrational normal modes weighted by Bose heat capacities. We show that this single kernel (1) produces apparent anisotropy $\Lambda_z \neq \Lambda_r$ as a consequence of the directional modal weights; (2) accounts for the TDTR conductivities of Si, Ge, and $\mathrm{Si}_{1-x}\mathrm{Ge}_x$ as a spatial-nonlocality effect set by $d_p(f)$: in its parameter-free relaxation-time closure, with first-principles-anchored MFP spectra, it reproduces the spot-size dependence and in-plane anisotropy of Si and the frequency dependence of Ge and $\mathrm{Si}_{0.2}\mathrm{Ge}_{0.8}$ (Secs. SIV B to SVIII of the Supplemental Material [27]); and (3) contains the two-channel ballistic/diffusive description of nondiffusive transport [10,12,42] as a two-sector projection.

Generalized constitutive relation. We extend the validity of the Gibbs equation to internal degrees of freedom $\boldsymbol{\Gamma} = (\mathbf{p}, \mathbf{r})$ that have not yet relaxed to local equilibrium. For a phase-space density $\rho(\boldsymbol{\Gamma}, t)$ of heat carriers, the entropy production rate is $\sigma = -\int \mathbf{J}_{\boldsymbol{\Gamma}} \cdot \boldsymbol{\nabla}_{\boldsymbol{\Gamma}}(\mu/T)\, d\boldsymbol{\Gamma} \geqslant 0$, with $\mu(\boldsymbol{\Gamma}, t)$ a nonequilibrium chemical potential [36,37]. Even in steady state, bosonic carriers can acquire a nonzero effective chemical potential, as in near-field photonic cooling [43] and nonequilibrium Casimir experiments [44].

Postulating a causal linear response in phase space consistent with $\sigma \geqslant 0$, and coarse graining onto the energy-density field, yields a generalized constitutive law for the macroscopic heat flux (see the Supplemental Material [27]),

$$\mathbf{J}_q(\mathbf{r},t) = \int_{-\infty}^{t} dt' \int d\mathbf{r}'\, \mathbf{L}_{qq}(\mathbf{r},\mathbf{r}',t-t')\, \nabla_{\mathbf{r}'}\left[\frac{1}{T(\mathbf{r}',t')}\right]. \tag{2}$$

The spatiotemporal kernel $\mathbf{L}_{qq}$ is not *ad hoc*: It arises from the projection of phase-space correlations connecting transport at $\mathbf{r}'$ to $\mathbf{r}$ through carrier propagation and scattering, and its symmetric part is positive semidefinite, guaranteeing $\sigma \geqslant 0$ [27]. Linearizing about a reference T_0 via $\nabla(1/T) \simeq -T_0^{-2}\nabla\delta T$ and Fourier transforming in space and time recasts Eq. (2) as a generalized Fourier law,

$$\mathbf{J}_q(\mathbf{k},\omega) = -i\,\boldsymbol{\kappa}_{\text{eff}}(\mathbf{k},\omega)\cdot\mathbf{k}\;\delta T(\mathbf{k},\omega), \tag{3}$$

with $\boldsymbol{\kappa}_{\text{eff}}(\mathbf{k},\omega) \equiv \widetilde{\mathbf{L}}_{qq}(\mathbf{k},\omega)/T_0^2$ the generalized conductivity tensor. The classical law, Eq. (1), is recovered strictly in the hydrodynamic limit $\mathbf{k}\to 0,\ \omega\to 0$, where the kernel reduces to a Dirac delta in space and time and $\boldsymbol{\kappa}_{\text{eff}} \to \kappa\,\mathbf{1}$. In TDTR, the surface response is a Hankel-space integral over in-plane wave vectors weighted by the beam profiles [13,45], so that the in-plane kernel enters that integral, $\kappa_r \to \kappa_{\text{eff}}^{rr}(k)$, without a single-wave-vector approximation (to leading order in k_z/k_r, away from the transducer interface); the dominant gradients are nevertheless set by $k_z \sim d_p^{-1}(f)$ through-plane and $k_r \sim w_0^{-1}$ in-plane, making the fitted local conductivities directional proxies for $\boldsymbol{\kappa}_{\text{eff}}(\mathbf{k})$ [10].

Modal kernel and anisotropy. To ground the kernel microscopically, we project the Liouville evolution of $\boldsymbol{\Gamma}$ onto a column vector $\mathbf{A}(t)$ of slow variables. The Mori-Kubo-Zwanzig identity yields the exact generalized Langevin equation (GLE) [27],

$$\frac{d\mathbf{A}(t)}{dt} = i\boldsymbol{\Omega}\,\mathbf{A}(t) - \int_0^t d\tau\;\boldsymbol{\Phi}(\tau)\,\mathbf{A}(t-\tau) + \mathbf{F}(t), \tag{4}$$

with $\boldsymbol{\Omega}$ the reversible frequency matrix, $\mathbf{F}(t)$ the projected stochastic force, and the memory kernel obeying the fluctuation-dissipation theorem $\boldsymbol{\Phi}(\tau) = \langle \mathbf{F}(\tau)\mathbf{F}^T(0)\rangle\,\mathbf{C}^{-1}$, $\mathbf{C} \equiv \langle \mathbf{A}\mathbf{A}^T\rangle$. The normalized propagator $\mathbf{R}(t) = \mathbf{C}(t)\mathbf{C}^{-1}$ has Laplace transform $\widetilde{\mathbf{R}}(z) = [z\mathbf{1} - i\boldsymbol{\Omega} + \widetilde{\boldsymbol{\Phi}}(z)]^{-1}$, whose poles set the mesoscopic timescales.

Choosing the components of $\mathbf{A}$ as the modal energy fluctuations $A_\mu(t) = \delta E_\mu(t) = \varepsilon_\mu[n_\mu(t) - n_\mu^{\text{eq}}]$ of the vibrational eigenmodes $\phi_\mu(\mathbf{r})$ of the confined medium (with $\varepsilon_\mu = \hbar\omega_\mu$), the heat flux separates into geometry and dynamics, $\mathbf{J}_q(\mathbf{r},t) = \sum_\mu \boldsymbol{\Psi}_\mu(\mathbf{r})A_\mu(t)$, with the *vectorial* mode flux functions

$$\boldsymbol{\Psi}_\mu(\mathbf{r}) = \mathbf{v}_\mu(\mathbf{r})\,|\phi_\mu(\mathbf{r})|^2 \tag{5}$$

carrying the directional group velocity $\mathbf{v}_\mu$. The Onsager kernel then follows in closed, tensor form [27],

$$L_{qq}^{ij}(\mathbf{r},\mathbf{r}',t) = T_0^2 \sum_{\mu,\nu} \Psi_\mu^i(\mathbf{r})\,\Psi_\nu^j(\mathbf{r}')\,R_{\mu\nu}(t)\,c_{\text{ph}}(\omega_\nu,T), \tag{6}$$

where the classical variance is replaced by the spectral (Bose) heat capacity

$$c_{\text{ph}}(\omega,T) = k_B\left(\frac{\hbar\omega}{2k_BT}\right)^2 \text{csch}^2\left(\frac{\hbar\omega}{2k_BT}\right). \tag{7}$$

Equation (6) is the central structural result. In a confined structure, spatial nonlocality is carried by the mode overlap $\Psi_\mu^i(\mathbf{r})\Psi_\nu^j(\mathbf{r}')$; in a bulk crystal, where $|\phi_\mu|^2$ is uniform, it is carried by the reversible streaming term $i\Omega_{\mu\nu}(\mathbf{k}) = -i\,\mathbf{k}\cdot\mathbf{v}_\mu\delta_{\mu\nu}$ of Eq. (4), so that $R_{\mu\nu}$ acquires a $\mathbf{k}$ dependence; temporal memory resides in the dissipative kernel $\boldsymbol{\Phi}$; and the quantum weight $c_{\text{ph}}(\omega_\nu,T)$ "freezes out" high-frequency modes for $k_BT \ll \hbar\omega_\nu$, correcting the systematic overestimate of heat flow by classical models below the Debye temperature [8,46], and coincides with the modal heat capacity

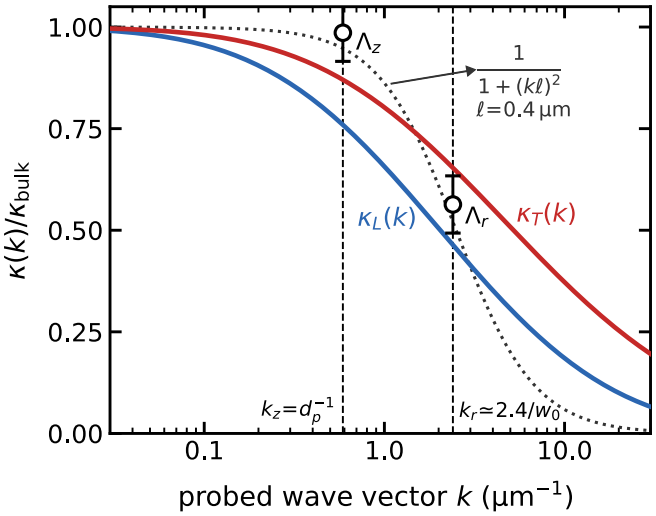


FIG. 1. Apparent anisotropy from a single nonlocal kernel. Longitudinal and transverse blocks $\kappa_L(k)$, $\kappa_T(k)$ of the relaxation-time kernel of Si at 300 K, Eqs. (6)–(8) with a first-principles-anchored MFP spectrum (Secs. SIV B and SVIII of the Supplemental Material [27]; no adjustable parameter), and the one-length Lorentzian of Eq. (10) with $\ell = 0.4$ μm (dotted). A TDTR experiment samples the through-plane direction at $k_z \simeq d_p^{-1}(f)$ and the in-plane direction at $k_r \simeq 2.4/w_0$ (dashed lines; $f = 9.8$ MHz, $w_0 = 1$ μm), so a nominally isotropic crystal yields $\Lambda_z \neq \Lambda_r$; symbols are the beam-offset values of Wilson and Cahill [10], normalized to the measured $\kappa_{\rm bulk} = 142$ W m^{-1} K^{-1} (the kernel to its own bulk value, 148 W m^{-1}K^{-1}). The through-plane point lies above $\kappa_L(k_z)$ because the Si response in that direction is interface dominated (Sec. SIV C of the Supplemental Material [27]).

C_μ of kinetic theory [22,26]. With the Markovian closure $\Phi_{\mu\nu} = 2\tau_\mu^{-1}\delta_{\mu\nu}\delta(t)$, Eqs. (4) and (6) give $\kappa_{\rm eff}^{ij}(\mathbf{k}) = V^{-1}\sum_\mu C_\mu v_\mu^i v_\mu^j \tau_\mu/[1 + (\mathbf{k}\cdot\mathbf{\Lambda}_\mu)^2]$, with $\mathbf{\Lambda}_\mu = \mathbf{v}_\mu\tau_\mu$ and V the volume, which is the nonlocal conductivity of the Boltzmann equation [14,22]; its longitudinal and transverse blocks are suppressed as $1 - \frac{3}{5}(k\Lambda)^2$ and $1 - \frac{1}{5}(k\Lambda)^2$ at long wavelength (Fig. 1; Sec. SIV B of the Supplemental Material; scope and limitations are provided in Sec. SVIII A of the Supplemental Material [27]). Distinct carrier families (acoustic and optical phonons, or internal radiation in translucent solids [11]) enter additively through disjoint mode sectors.

The tensor structure of Eq. (6) has an immediate, testable consequence. Fourier transforming in space and time, the diagonal blocks of the conductivity read

$$\kappa_{\rm eff}^{ii}(\mathbf{k},\omega) = \frac{1}{V}\sum_{\mu,\nu}\widetilde{\Psi}_\mu^i(\mathbf{k})\,\widetilde{\Psi}_\nu^i(-\mathbf{k})\,\widetilde{R}_{\mu\nu}(\mathbf{k},\omega)\,c_{\rm ph}(\omega_\nu,T), \tag{8}$$

where the mode overlap (confined modes) or the streaming propagator $\widetilde{R}_{\mu\nu}(\mathbf{k},\omega)$ (bulk) is maximal at $\mathbf{k}\to 0$ and is cut off for $|\mathbf{k}| \gtrsim \ell^{-1}$, so each block decreases monotonically with $|\mathbf{k}|$. Because $\mathbf{\Psi}_\mu$ points along the mode group velocity, the kernel is a tensor whose blocks a TDTR experiment samples at direction-dependent wave vectors, $k_z \simeq d_p^{-1}(f) = \sqrt{\pi C f/\kappa_{\rm ref}}$ and $k_r \simeq c/w_0$ ($c \simeq 2.3$–2.4 for the beam-offset width at $w_0 \approx 1$–1.5 μm, rising slowly with w_0; Sec. SVIII of the Supplemental Material [27]); this sampling yields, in the absence of interfacial effects,

$$\Lambda_z = \kappa_{\rm eff}^{zz}\big(k_z \sim d_p^{-1}\big) \neq \Lambda_r = \kappa_{\rm eff}^{rr}(k_r \sim c/w_0), \tag{9}$$

with the more strongly sampled direction the more suppressed (Fig. 1). For Si at $w_0 \approx 1$ μm and $f = 9.8$ MHz, with $\kappa_{\rm ref} \approx 142$ W m^{-1} K^{-1} (taken as the bulk value) and $C \approx 1.6\times10^6$ J m^{-3} K^{-1}, one finds $d_p \approx 1.7$ μm, hence $k_z \approx 0.6 < k_r \approx 2.4$ μm^{-1} and $\Lambda_r < \Lambda_z$, in qualitative

agreement with the beam-offset values quoted above: A nominally isotropic kernel produces apparent anisotropy purely through direction-dependent sampling. Raising f shifts k_z outward and suppresses the through-plane channel; shrinking w_0 shifts k_r outward and suppresses the in-plane channel, reproducing the experimentally observed selectivity of the two knobs [10]. Inserting this parameter-free relaxation-time kernel, built from a first-principles-anchored MFP spectrum, into the multilayer TDTR model [13,45] reproduces both the pump-diameter dependence $\Lambda_A(D)$ of Ding *et al.* [21] ($121 \to 148$ W m^{-1} K^{-1} versus $115 \to 143$ W m^{-1} K^{-1} for $D = 3.7 \to 60$ μm) and the beam-offset Λ_r at $w_0 = 1$ μm (70–92 W m^{-1} K^{-1}, depending on the MFP spectrum, versus 80 W m^{-1} K^{-1}) [Figs. S1(b) and S1(c) and Sec. SVIII of the Supplemental Material [27]], whereas through-plane transport in Si is governed by the interfacial condition (below).

Limiting cases. For a bath spectral density $S(\omega) \propto \omega^s$, $\widetilde{\mathbf{\Phi}}(z) \sim z^{s-1}$ classifies normal ($s = 1$), anomalous ($0 < s < 2, s \neq 1$), and ballistic ($s = 2$) transport (Sec. SV of the Supplemental Material [27,47–51]). A Markovian kernel $\mathbf{\Phi}(t) \approx 2\tau_q^{-1}\mathbf{1}\,\delta(t)$ makes the flux correlations exponential, i.e., gives $\widetilde{\mathbf{R}}(z)$ a single inertial pole at $z = -\tau_q^{-1}$: For $\omega\tau_q \ll 1$, it recovers Fourier's law (and, with streaming, the Boltzmann kernel above), while retaining the pole yields the Cattaneo-Vernotte equation [52,53] $\tau_q \partial_t \mathbf{J}_q + \mathbf{J}_q = -\kappa \nabla T$, whose spatial counterpart is the Guyer-Krumhansl kernel [26,54]. Temporal memory ($\omega\tau_q \sim 1$) thus governs second sound, whereas TDTR and room-temperature transient gratings [12] operate on timescales far longer than τ_q.

Spatial nonlocality and the TDTR data. To lowest order in gradients, the isotropic nonlocal conductivity is represented by a minimal one-length ansatz, a Lorentzian in wave vector,

$$\kappa_{\mathrm{eff}}(k) = \frac{\kappa_{\mathrm{bulk}}}{1 + (k\ell)^2}, \tag{10}$$

which is the [0/1] Padé closure consistent with the long-wavelength expansion of a finite-range spatial kernel (Sec. SIV A of the Supplemental Material [27]); in the relaxation-time closure $\ell^2 = \frac{3}{5}\langle\Lambda^2\rangle_\kappa$, with $\langle\Lambda^2\rangle_\kappa$ the κ-weighted second moment of the MFP spectrum, but for broad spectra the full kernel decays almost logarithmically in k (Fig. 1), so that Eq. (10) is an effective one-length description over the measured decade.

Evaluated at $k_z = d_p^{-1}$, this gives a frequency-resolved apparent conductivity

$$\Lambda_A(f) = \frac{\kappa_{\mathrm{bulk}}}{1 + f/f^*}, \quad f^* = \frac{\kappa_{\mathrm{ref}}}{\pi C\,\ell^2}, \tag{11}$$

controlled by a single effective length ℓ rather than a relaxation time. The crossover frequency f^* is large (response flat) when ℓ is short, and small (early roll-off) when ℓ is long.

Figure 2 compares Eq. (11) with the apparent conductivities of Wilson and Cahill [10] over $f = 1$–20 MHz. Fitting κ_{bulk} and f^* per material (C fixed, ℓ derived from f^*) matches every dataset ($\chi^2_\nu < 1$); with six points over one decade, this is a consistency check of an effective one-length description, not a stand-alone test of the theory, which rests on the parameter-free calculations of Fig. 1 and Figs. S1 and S2 of the Supplemental Material [27]. Pure Si and boron-doped Si (Si:B) remain flat ($d_p \gg \ell$; $\ell_{\mathrm{Si}} \lesssim 0.6$ μm at 1σ), while Ge and the SiGe alloys roll off, yielding $\ell_{\mathrm{Ge}} = 0.41 \pm 0.09$ μm, $\ell_{\mathrm{Si_{0.99}Ge_{0.01}}} = 0.34 \pm 0.07$ μm, and $\ell_{\mathrm{Si_{0.2}Ge_{0.8}}} = 0.25 \pm 0.04$ μm (1σ statistical; systematic ± 0.15 μm from the functional form and the treatment of κ_{bulk}; Sec. SVI A and Table S1 of the Supplemental Material [27]). Within this one-length description, the trend across materials is transparent in Eq. (6): Mass-disorder scattering [55] ($\propto \omega^4$) removes high-frequency modes and *increases* the fraction of κ carried by long-MFP modes (from 24% to 47% above 1 μm when 1% Ge is added to Si; Sec. SVIII of the Supplemental Material [27]), while the lower alloy conductivity shrinks d_p and pushes $k_z = d_p^{-1}$ deeper into the nonlocal regime, so that ℓ reflects the MFP window sampled by $d_p(f)$ [10,56]. Solving the through-plane boundary-value problem directly with the modal kernel (Sec. SIV C and Fig. S2 of the Supplemental Material [27]) reproduces $\Lambda_A(f)$ of Ge and $\mathrm{Si_{0.2}Ge_{0.8}}$ without adjustable parameters under an interface condition adiabatic below 3 THz [25] ($\mathrm{Si_{0.99}Ge_{0.01}}$ falling between this condition and a fully thermalizing interface); for Si, the

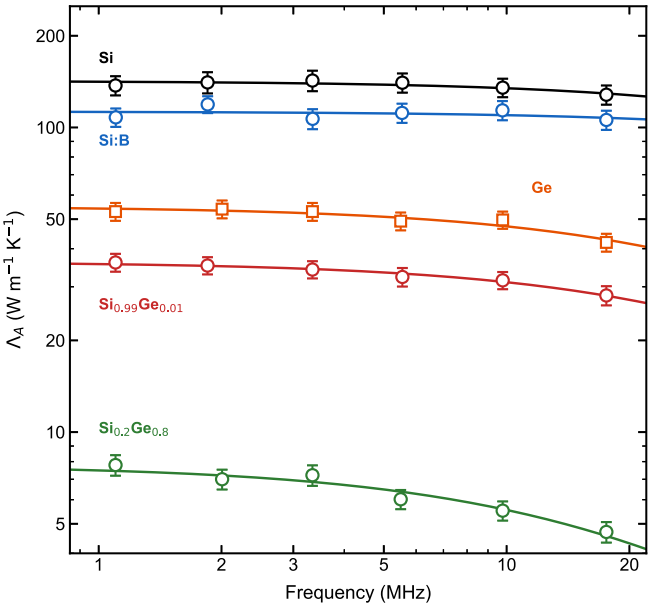


FIG. 2. Apparent thermal conductivity Λ_A vs modulation frequency: TDTR data of Wilson and Cahill [10] [symbols, with error bars; digitized from their Fig. 3(a) at $w_0 = 10$ μm] and two-parameter fits of Eq. (11) (solid lines). Fourier's law predicts a constant Λ_A; Si and Si:B stay flat while Ge and the SiGe alloys are suppressed at high f, where the shrinking penetration depth $d_p(f)$ probes a larger wave vector. The effective lengths are $\ell = 0.41$, 0.34, and 0.25 μm for Ge, $Si_{0.99}Ge_{0.01}$, and $Si_{0.2}Ge_{0.8}$, respectively. Parameter-free kernel calculation of the same data and of the apparent interface conductance $G_A(f)$: Fig. S2 of the Supplemental Material [27].

bulk kernel alone overpredicts the through-plane suppression by an amount set by the fraction of κ in long-MFP modes (19% or 13% decline over the band for 40% or 24% of κ above 1 μm, against 7% ± 8% measured), the flat $\Lambda_z(f)$ being controlled by the Al/Si interface [22] and by the amplitude-phase compensation of the out-of-phase signal [15].

Role of the interface. The same modal picture clarifies why a local boundary conductance is insufficient [10]. Near a metal/sample boundary, the reflected and transmitted modes truncate the overlap $\Psi^i_\mu(\mathbf{r})\Psi^j_\nu(\mathbf{r}')$ within a layer of thickness set by the MFP, leaving residual off-diagonal correlations $R_{\mu\nu}$ ($\mu \neq \nu$) that do not relax to a single local temperature. In the language of Eq. (6), the short- and long-MFP sectors are driven out of mutual equilibrium over a finite length, which is precisely the interfacial nonequilibrium resistance inferred phenomenologically from the frequency dependence of the apparent interface conductance in SiGe alloys [10,25]. Projecting Eq. (4) onto a long-MFP sector and a diffusive reservoir recovers the two-channel model of Ref. [25] and maps its nonequilibrium length $d \simeq 150$ nm onto the range of the ballistic sector, $\ell_1 = d\sqrt{(\Lambda_1 + \Lambda_2)/\Lambda_2} \simeq 0.28$ μm, with $\Lambda_{1,2}$ the conductivities of the two channels (Sec. SVII of the Supplemental Material [27]). For a thermalizing interface, the boundary-value solution (Sec. SIV C of the Supplemental Material [27]) yields the excess resistance $R_{\rm neq} = \Delta T_{\rm neq}/q''$, the additional interfacial temperature drop per unit heat flux q'' that a local model must assume: $\approx 6.5 \times 10^{-9}\,\mathrm{m^2\,K\,W^{-1}}$ at 1 MHz for $Al/Si_{0.99}Ge_{0.01}$ (3.0 and 2.5×10^{-9} for Si and Ge). This is comparable to measured interface (Kapitza) resistances ($3–7 \times 10^{-9}\,\mathrm{m^2\,K\,W^{-1}}$ for Al/Si and Al/SiGe [20,22,25]) and decreases with f, reproducing the frequency increment, though not the absolute level, of the rise of the apparent interface conductance $G_A(f)$ that accompanies the drop of $\Lambda_A(f)$ [25] (Fig. S2(b) of the Supplemental Material [27]). The kernel thus places the diffusive reservoir and the nonlocal ballistic channel of the two-fluid description [12,42] on a common, entropy-producing footing, rather than positing them separately.

Conclusion. We have derived a thermodynamically consistent generalization of Fourier's law in which the conductivity is a nonlocal memory operator $\boldsymbol{\kappa}_{\rm eff}(\mathbf{k}, \omega)$, whose Onsager kernel decomposes into vibrational normal modes weighted by Bose heat capacities and relaxation functions [Eq. (6)]. The kernel is a tensor even in a cubic crystal, and direction-dependent sampling of it yields apparent anisotropy $\Lambda_z \neq \Lambda_r$ in a nominally isotropic crystal; the recognition that TDTR samples $\boldsymbol{\kappa}_{\rm eff}$ at a frequency-set wave vector $k_z \sim d_p^{-1}$ recasts the measured suppression in Ge and SiGe as spatial nonlocality, described by an effective length $\ell \simeq 0.25$–0.4 μm and, without adjustable parameters, by the relaxation-time kernel with the interfacial condition on the long-MFP modes; for the through-plane response of Si, the kernel alone overpredicts the suppression and the interface condition dominates; and the truncation of modal overlaps at a boundary provides a microscopic origin for the interfacial nonequilibrium resistance. Together, these results place the two-channel ballistic/diffusive picture on a thermodynamic and microscopic footing [10,12,25,42], and recover the relaxation-time kernel of the Boltzmann equation as the Markovian closure of the GLE. Relative to BTE-based and hydrodynamic analyses of TDTR [15,21,22,24], the framework adds a second law that holds for any closure consistent with the fluctuation-dissipation theorem and non-Markovian memory; relative to the Green-Kubo kernel of Ref. [26], which shares its positivity and its Guyer-Krumhansl limit, it adds the thermodynamic (MNET) route, the fluctuation-dissipation structure of the memory function, and an interface resistance computed from the same kernel, given a modal boundary condition, rather than from a separate interfacial kernel; and it does not replace the first-principles input (lifetimes, transmissivities) on which those analyses rely and which it consumes unchanged. Three predictions follow (Sec. SX of the Supplemental Material [27]): For the same in-plane wave vector, the apparent in-plane suppression should exceed the through-plane one by a factor of 1.5–2 for $w_0 = 1$–10 μm (bounded by 3 at long wavelength) in a material whose through-plane response is not interface dominated; Λ_r measured with different spot sizes and geometries should collapse on the single curve $\kappa_L(k)$ once each geometry is mapped to its effective wave vector by the forward model ($k \simeq 2.3/w_0$ at $w_0 = 1$ μm, $3.6/w_0$ at 10 μm); and isotopically enriched ^{28}Si should show the same Λ_r as natural Si at $w_0 = 1$ μm despite an 8% larger $\kappa_{\rm bulk}$. Because the kernel is expressed through equilibrium correlation functions and modal heat capacities, the framework connects experimental observables to microscopic parameters without *ad hoc* extensions and applies directly to nanowires, superlattices, and quantum dots, to the temperature dependence of nondiffusive transport through $c_{\rm ph}(\omega, T)$, and, by extension to electronic variables, to thermoelectric and active quantum devices [57].

Acknowledgments. The author gratefully acknowledges the financial support by National Institute of Science and Technology in Innovative Research in Health Sciences—from Nanotechnology to Artificial Intelligence (INCT PICS) sponsored by Brazil's National Council for Scientific and Technological Development (CNPq), Grant No. 408417/2024-2.

Data availability. There are no publicly available research data or software supporting this manuscript. Requests for further information or data should be sent to the author.

[1] G. Chen, *Nanoscale Energy Transport and Conversion: A Parallel Treatment of Electrons, Molecules, Phonons, and Photons* (Oxford University Press, New York, 2005).

[2] J.-J. Greffet, Electrons and phonons, in *Microscale and Nanoscale Heat Transfer*, edited by S. Volz (Springer, Berlin, 2007), pp. 37–54.

[3] J. B. J. Fourier, *Théorie Analytique de la Chaleur* (Didot, Paris, 1822).

[4] J.-J. Greffet, Laws of macroscopic heat transfer and their limits, in *Microscale and Nanoscale Heat Transfer*, edited by S. Volz (Springer, Berlin, 2007), pp. 1–13.

[5] D. Bimberg, M. Grundmann, and N. N. Ledentsov, *Quantum Dot Heterostructures* (John Wiley & Sons, Chichester, 1999).
[6] B. J. Berne and R. Pecora, *Dynamic Light Scattering: With Applications to Chemistry, Biology, and Physics* (Dover, New York, 2000).
[7] B. Alberts, R. Heald, A. Johnson, D. Morgan, M. C. Raff, K. Roberts, and P. Walter, *Molecular Biology of the Cell* (W. W. Norton & Company, New York, 2022).
[8] D. G. Cahill, W. K. Ford, K. E. Goodson, G. D. Mahan, A. Majumdar, H. J. Maris, R. Merlin, and S. R. Phillpot, Nanoscale thermal transport, J. Appl. Phys. **93**, 793 (2003).
[9] J. A. Johnson, A. A. Maznev, J. Cuffe, J. K. Eliason, A. J. Minnich, T. Kehoe, C. M. Torres, G. Chen, and K. A. Nelson, Direct measurement of room-temperature nondiffusive thermal transport over micron distances in a silicon membrane, Phys. Rev. Lett. **110**, 025901 (2013).
[10] R. B. Wilson and D. G. Cahill, Anisotropic failure of Fourier theory in time-domain thermoreflectance experiments, Nat. Commun. **5**, 5075 (2014).
[11] K. Zheng, S. Ghosh, and S. Granick, Exceptions to Fourier's law at the macroscale, Proc. Natl. Acad. Sci. USA **121**, e2320337121 (2024).
[12] A. A. Maznev, J. A. Johnson, and K. A. Nelson, Onset of nondiffusive phonon transport in transient thermal grating decay, Phys. Rev. B **84**, 195206 (2011).
[13] J. P. Feser and D. G. Cahill, Probing anisotropic heat transport using time-domain thermoreflectance with offset laser spots, Rev. Sci. Instrum. **83**, 104901 (2012).
[14] G. D. Mahan and F. Claro, Nonlocal theory of thermal conductivity, Phys. Rev. B **38**, 1963 (1988).
[15] Y. K. Koh, D. G. Cahill, and B. Sun, Nonlocal theory for heat transport at high frequencies, Phys. Rev. B **90**, 205412 (2014).
[16] C. Hua and A. J. Minnich, Analytical Green's function of the multidimensional frequency-dependent phonon Boltzmann equation, Phys. Rev. B **90**, 214306 (2014).
[17] P. B. Allen and V. Perebeinos, Temperature in a Peierls-Boltzmann treatment of nonlocal phonon heat transport, Phys. Rev. B **98**, 085427 (2018).
[18] C. Hua and L. Lindsay, Space-time dependent thermal conductivity in nonlocal thermal transport, Phys. Rev. B **102**, 104310 (2020).
[19] F. Yang and C. Dames, Heating-frequency-dependent thermal conductivity: An analytical solution from diffusive to ballistic regime and its relevance to phonon scattering measurements, Phys. Rev. B **91**, 165311 (2015).
[20] A. J. Minnich, J. A. Johnson, A. J. Schmidt, K. Esfarjani, M. S. Dresselhaus, K. A. Nelson, and G. Chen, Thermal conductivity spectroscopy technique to measure phonon mean free paths, Phys. Rev. Lett. **107**, 095901 (2011).
[21] D. Ding, X. Chen, and A. J. Minnich, Radial quasiballistic transport in time-domain thermoreflectance studied using Monte Carlo simulations, Appl. Phys. Lett. **104**, 143104 (2014).
[22] C. Hua, L. Lindsay, X. Chen, and A. J. Minnich, Generalized Fourier's law for nondiffusive thermal transport: Theory and experiment, Phys. Rev. B **100**, 085203 (2019).
[23] A. Beardo, S. Alajlouni, L. Sendra, J. Bafaluy, A. Ziabari, Y. Xuan, J. Camacho, A. Shakouri, and F. X. Alvarez, Hydrodynamic thermal transport in silicon at temperatures ranging from 100 to 300 K, Phys. Rev. B **105**, 165303 (2022).
[24] Z. Xiang, P. Jiang, and R. Yang, Time-domain thermoreflectance (TDTR) data analysis using phonon hydrodynamic model, J. Appl. Phys. **132**, 205104 (2022).
[25] R. B. Wilson, J. P. Feser, G. T. Hohensee, and D. G. Cahill, Two-channel model for nonequilibrium thermal transport in pump-probe experiments, Phys. Rev. B **88**, 144305 (2013).
[26] Y. Zeng and J. Dong, Unified statistical theory of heat conduction in nonuniform media, Phys. Rev. B **113**, 235204 (2026).
[27] See Supplemental Material at http://link.aps.org/supplemental/10.1103/ggz5-nggb for the derivation of the constitutive law, the generalized Langevin equation and the modal Onsager kernel, its relaxation-time closure and tensor structure, the through-plane boundary-value problem and the interfacial nonequilibrium resistance, the mean-free-path spectra and thermoreflectance forward model, the fitting procedure and

uncertainties, a comparison with previous treatments, and testable predictions, which includes Refs. [28–34].
[28] L. Onsager, Reciprocal relations in irreversible processes. I, Phys. Rev. **37**, 405 (1931).
[29] L. Onsager, Reciprocal relations in irreversible processes. II, Phys. Rev. **38**, 2265 (1931).
[30] K. Esfarjani, G. Chen, and H. T. Stokes, Heat transport in silicon from first-principles calculations, Phys. Rev. B **84**, 085204 (2011).
[31] K. T. Regner, D. P. Sellan, Z. Su, C. H. Amon, A. J. H. McGaughey, and J. A. Malen, Broadband phonon mean free path contributions to thermal conductivity measured using frequency domain thermoreflectance, Nat. Commun. **4**, 1640 (2013).
[32] S.-I. Tamura, Isotope scattering of dispersive phonons in Ge, Phys. Rev. B **27**, 858 (1983).
[33] J. Carrete, B. Vermeersch, A. Katre, A. van Roekeghem, T. Wang, G. K. H. Madsen, and N. Mingo, almaBTE: A solver of the space–time dependent Boltzmann transport equation for phonons in structured materials, Comput. Phys. Commun. **220**, 351 (2017).
[34] B. Vermeersch, J. Carrete, N. Mingo, and A. Shakouri, Superdiffusive heat conduction in semiconductor alloys. I. Theoretical foundations, Phys. Rev. B **91**, 085202 (2015).
[35] S. R. de Groot and P. Mazur, *Non-Equilibrium Thermodynamics* (Dover, New York, 1984).
[36] J. M. G. Vilar and J. M. Rubí, Thermodynamics "beyond" local equilibrium, Proc. Natl. Acad. Sci. USA **98**, 11081 (2001).
[37] D. Reguera, J. M. Rubí, and J. M. G. Vilar, The mesoscopic dynamics of thermodynamic systems, J. Phys. Chem. B **109**, 21502 (2005).
[38] H. Mori, Transport, collective motion, and Brownian motion, Prog. Theor. Phys. **33**, 423 (1965).
[39] R. Kubo, Statistical-mechanical theory of irreversible processes. I. General theory and simple applications to magnetic and conduction problems, J. Phys. Soc. Jpn. **12**, 570 (1957).
[40] R. Zwanzig, Memory effects in irreversible thermodynamics, Phys. Rev. **124**, 983 (1961).
[41] R. Zwanzig, *Nonequilibrium Statistical Mechanics* (Oxford University Press, New York, 2001).
[42] B. H. Armstrong, Two-fluid theory of thermal conductivity of dielectric crystals, Phys. Rev. B **23**, 883 (1981).
[43] L. Zhu, A. Fiorino, D. Thompson, R. Mittapally, E. Meyhofer, and P. Reddy, Near-field photonic cooling through control of the chemical potential of photons, Nature (London) **566**, 239 (2019).
[44] K. Chen and S. Fan, Nonequilibrium Casimir force with a nonzero chemical potential for photons, Phys. Rev. Lett. **117**, 267401 (2016).
[45] D. G. Cahill, Analysis of heat flow in layered structures for time-domain thermoreflectance, Rev. Sci. Instrum. **75**, 5119 (2004).
[46] K. Schwab, E. A. Henriksen, J. M. Worlock, and M. L. Roukes, Measurement of the quantum of thermal conductance, Nature (London) **404**, 974 (2000).
[47] R. Morgado, F. A. Oliveira, G. G. Batrouni, and A. Hansen, Relation between anomalous and normal diffusion in systems with memory, Phys. Rev. Lett. **89**, 100601 (2002).
[48] L. C. Lapas, I. V. L. Costa, M. H. Vainstein, and F. A. Oliveira, Entropy, non-ergodicity and non-Gaussian behaviour in ballistic transport, Europhys. Lett. **77**, 37004 (2007).
[49] M. H. Vainstein, I. V. L. Costa, R. Morgado, and F. A. Oliveira, Non-exponential relaxation for anomalous diffusion, Europhys. Lett. **73**, 726 (2006).
[50] L. C. Lapas, R. Morgado, M. H. Vainstein, J. M. Rubí, and F. A. Oliveira, Khinchin theorem and anomalous diffusion, Phys. Rev. Lett. **101**, 230602 (2008).
[51] E. G. Flekkøy, A. Hansen, and B. Baldelli, Hyperballistic superdiffusion and explosive solutions to the non-linear diffusion equation, Front. Phys. **9**, 640560 (2021).
[52] C. Cattaneo, Sulla conduzione del calore, Atti Semin. Mat. Fis. Univ. Modena **3**, 83 (1948).
[53] P. Vernotte, La véritable équation de la chaleur, C. R. Hebd. Séances Acad. Sci. **247**, 2103 (1958).
[54] R. A. Guyer and J. A. Krumhansl, Thermal conductivity, second sound, and phonon hydrodynamic phenomena in nonmetallic crystals, Phys. Rev. **148**, 778 (1966).

[55] Y. K. Koh and D. G. Cahill, Frequency dependence of the thermal conductivity of semiconductor alloys, Phys. Rev. B **76**, 075207 (2007).

[56] A. J. Minnich, Advances in the measurement and computation of thermal phonon transport properties, J. Phys.: Condens. Matter **27**, 053202 (2015).

[57] M. S. Gomes-Filho, L. C. Lapas, E. Gudowska-Nowak, and F. A. Oliveira, The fluctuation–dissipation relations: Growth, diffusion, and beyond, Phys. Rep. **1141**, 1 (2025).